Measurement 141 (2019) 217–226

Contents lists available at ScienceDirect

Measurement

journal homepage: www.elsevier.com/locate/measurement

Adaptive sliding mode control of maglev system based on RBF neural network minimum parameter learning method

Yougang Sun [a,b], Junqi Xu [b,*], Haiyan Qiang [b,c], Chen Chen [a,b], GuoBin Lin [a,b]

[a] College of Transportation Engineering, Tongji University, 201804, China
[b] National Maglev Transportation Engineering R&D Center, Tongji University, 201804, China
[c] College of Logistics Engineering, Shanghai Maritime University, 201306, China

ARTICLE INFO

Article history:
Received 14 October 2018
Received in revised form 6 December 2018
Accepted 3 March 2019
Available online 17 April 2019

Keywords:
Maglev system
Radial basis function (RBF)
Neural network
Minimum parameter learning
Adaptive sliding mode control

ABSTRACT

The electromagnet levitation control system is the core component of maglev trains, which has a significant influence on the performance of the maglev train. However, the control system suffers from the essential strong nonlinear and open-loop unstable. Moreover, the model uncertainty and many exogenous disturbances make the controller design even harder. In this paper, the mathematical model of maglev system is established firstly. Then, using the nonlinear transformation method, the affine nonlinear mathematical model of the maglev system is obtained without any linear approximation. Based on the presented model, we design a sliding mode controller based on the exponential reaching law preliminarily and the stability is proved. Since the control characteristics of the maglev system are highly uncertain and time varying with external disturbance, a radial basis function (RBF) neural network estimator is added to the proposed controller. To improve the convergence speed and better satisfy the requirements of real-time control, the minimum parameter learning method is adopted to replace the weights in the neural network without model information. The boundedness and convergence of the presented control law are proved by Lyapunov method. Finally, both simulation and experiment results are included to verify the effectiveness of the proposed control strategy.

1. Introduction

Maglev train is a modern means of transport with contactless electromagnetic levitation, guidance and drive systems. It relies on electromagnetic attraction or electric repulsion to suspend the train in the air to realize no mechanical contact between the train and the track, and driven by linear motors [1–4]. Maglev train is an ideal form of transport because of its fast speed, low energy consumption, comfortable ride and low noise. For EMS maglev train, the magnetic levitation system is the key and core of the maglev train [5]. However, the levitation system has strong nonlinearity and open-loop instability. Moreover, the system parameters are easy to change, and the system suffers from external disturbance during running [6,7]. Therefore, it proposes a high challenge to the design of maglev controller with high performance.

In recent years, the stability control of maglev train has attracted extensive attention from researchers all over the world, and obtained some achievements in the control methods. The conventional levitation control method of maglev train needs to conduct the first-order Taylor series expansion at the equilibrium point of the system, and then the control law is designed by utilizing the linear control method [8–11]. However, the levitation system of maglev train is a strong nonlinear system. Once the train is disturbed or the parameters of the system are changed, the control performance of the maglev system is easily reduced or even destabilized. Because the reference air gap of maglev train is very small, which is about 7–10 mm, the deterioration of this control performance is likely to lead to safety accidents. With the improvement of people's requirement for comfort of transportation, there are more and more requirements to improve the robustness, dynamics and overall performance of the maglev system. In recent years, advanced control method such as nonlinear control [12,13], fuzzy control [14–16], and sliding mode control [17] have been applied to maglev system. Many novel control methods for magnetic levitation system of maglev train have been proposed in many literatures. Sun et al. [18] proposed a novel controller based on repetitive learning to identify the external disturbance of maglev train, which effectively restrained the influence of exogenous disturbance. However, the factors such parameters perturbations are simplified to external disturbances. Yang et al. [19] designed

* Corresponding author at: National Maglev Transportation Engineering R&D Center, Tongji University, 201804, China.
E-mail address: xujunqi@tongji.edu.cn (J. Xu).

https://doi.org/10.1016/j.measurement.2019.03.006
0263-2241/

the controller of magnetic levitation system based on robust control. The overall response speed of the system is fast, and the system has good dynamic and steady-state performance, but the influence of robust control on the stability of the system is ordinary. Sun et al. [20] presented a fuzzy H∞ robust controller for magnetic levitation system based on T-S model, the simulation and experiment results showed the novel control strategy can solve the problems of model uncertainty and exogenous disturbances simultaneously. Huang [21] presented an adaptive controller based on backstepping method to provide system stability under model uncertainty, and achieves the desired suspension performance. Gutierrez et al. [22] proposed a MIMO control method with a high gain observer based on sliding mode for EDS MAGLEV. Xu et al. [23] analyzed the dynamics of maglev train of double delay and presented a theory to judge Hopf bifurcation of maglev system. But the control strategy to restrain the vibration has not been designed. Sun et al. [24] analyzed the nonlinear characteristics of the maglev system and proposed a fuzzy sliding mode controller to enhancing the anti-disturbance ability and carrying capacity of the maglev train. Xu et al. [25] presented a magnetic flux observer to design an adaptive sliding mode controller for magnetic levitation system of maglev train. Shen et al. [26] realized stable suspension of the maglev system based on sliding mode control. This method has the advantages of fast response, insensitivity to disturbances and easy implementation. However, high frequency chattering will reduce the control performance of the system, and even cause instability of the system.

Above all, the most urgent issues that the maglev system faces now are model uncertainty and exogenous disturbances, such as the uncertainty of the passenger weight, wind disturbance, and irregularities of the rail. At present, the commercial magnetic levitation controller for maglev vehicle is linear PID controller. When the parameters change or the external disturbance is large, the system will have slower response speed, larger overshoot, vibration and even lose stability under the current linear controller. Aiming at these problems, an adaptive sliding mode control law based on RBF neural network minimum parameter learning method (RBF MPL-ASMC) is proposed to deal with external disturbances, nonlinearity and parameter uncertainties. H. Morioka et al [27] have used neural network to realize online estimates about nonlinear part, uncertain part and unknown external interference in linear system and realized the equivalent control based on neural network. S.J. Huang et al.[28] have utilized neural network approximation ability to design the sliding mode control based on RBF neural network which uses switching functions as the input and controller is implemented entirely by continuous RBF function. In recent years, RBF neural network has been one of the hottest research methods, and gets some results. But, the convergence speed and real-time performance of RBF network limit its application on the maglev systems. There are few studies on RBF neural network control for the maglev train. So, in this paper, the minimum parameter learning method is adopted to replace the weights in the neural network without model information, and the adaptive control based on the minimum parameter estimation is realized, thereby improving the convergence speed of the adaptive algorithm and better meeting the requirements of real-time control.

The main contributions of the paper are as follows. We establish a mathematical model of maglev system firstly and then obtain an affine nonlinear mathematical model without any linear approximation through the nonlinear transformation method. Then, based on the affine nonlinear mathematical model and the exponential reaching law, a sliding mode controller design along with stability analysis is presented. After that, the RBF neural network with minimum parameter learning method is proposed to construct RBF MPL-ASMC controller to approximate unknown functions in the model. The boundedness and convergence of the control algorithm are proved by Lyapunov theorem. In the end, the effectiveness of the proposed control strategy is verified by both simulations and experiments. The proposed RBF MPL-ASMC has more excellent stable levitation effect in the magnetic suspension system of maglev train with system parameters perturbation and exogenous disturbance

The rest of this paper is organized as follows. In Section 2, the mathematical model of maglev system is established. Section 3 designs the adaptive sliding mode controller based on RBF neural network minimum parameter learning law (RBF MPL-ASMC). Section 4 implements the convergence analysis and the proof of uniformly ultimate boundedness. Simulation and experiment results are shown in Sections 5 and 6, respectively. Finally, the conclusions and future work directions are drawn in Section 7.

2. Dynamics of maglev system

The structure of maglev system of the train is shown in Fig. 1. Through structure decoupling of maglev bogie, the maglev system can be decomposed into a single electromagnet levitation system [29]. Taking the single electromagnet system as control object is more versatile to design a control law for the maglev train [30–33]. Thus, the electromagnet levitation system of maglev train is simplified into a single-magnetic levitation model as illustrated in Fig. 2. mg represents the load and self-gravity of levitation magnet, $x_m(t)$ denotes the airgap between the electromagnet and the rail, x_{ref} and Δx are reference airgap and airgap error, respectively, N_m denotes the turns number of the magnetic coil , A_m denotes the sectional area of Magnet, $u_m(t)$ and $i_m(t)$ represent the voltage and current in the magnetic coil, respectively,R_m denotes the coil resistance, and $L_M(x_m(t))$ is the inductance of the electromagnetic coil.

According to Maxwell's equation and Biot-Savar's theorem:

$$F_m(i_m(t), x_m(t)) = \frac{\int_0^t \psi_m(i_m(t), x_m(t))dt}{\partial x_m(t)} \tag{1}$$

Ignore the leakage flux of the electromagnet winding, then $\phi_L = 0$. According to the Kirchhoff law of the magnetic circuit:

$$\psi_m(i_m(t), x_m(t)) = N_m \frac{N_m i_m(t)}{R(x_m)} \tag{2}$$

where, $R(x_m)$ can be expressed as:

$$R(x_m) = \frac{2x_m(t)}{\mu_0 A_m} \tag{3}$$

Substituting Eqs. (2) and (3) into Eq. (1) can obtain the electromagnetic force equation of the magnetic levitation system as:

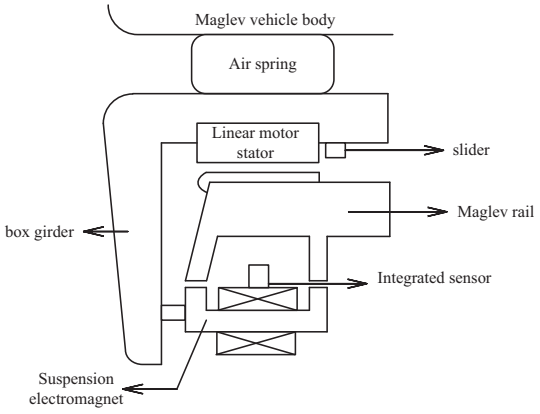

Fig. 1. Structure of Maglev system.

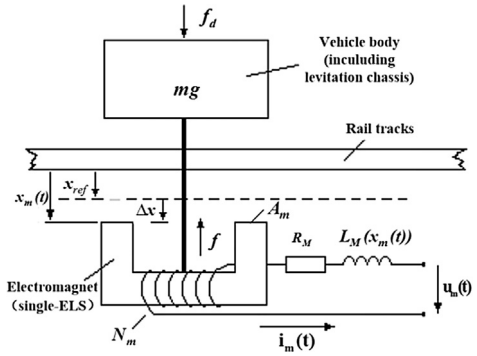

Fig. 2. The single-electromagnet system.

$$F_m(i_m(t),x_m(t)) = -\frac{\mu_0 A_m N_m^2}{4}\left[\frac{i_m(t)}{x_m(t)}\right]^2 \tag{4}$$

The relationship between voltage and current across the solenoid coil is:

$$u_m(t) = i_m(t)R_m + N_m\dot{\phi}_m \tag{5}$$

where, L_m is the instantaneous inductance of the electromagnet, which can be expressed as:

$$L_m = \frac{\mu_0 N_m^2 A_m}{2x_m(t)},\ \phi_m = \frac{L_m}{N_m} i_m(t) \tag{6}$$

Finishing (6) and deriving its time at both ends:

$$\dot{\phi}_m = \frac{\mu_0 N_m A_m}{2x_m(t)}\frac{di_m(t)}{dt} - \frac{\mu_0 N_m A_m i_m(t)}{2x_m^2(t)}\frac{dx_m(t)}{dt} \tag{7}$$

By the formula (5) and (7) can get electrical equation of electromagnet:

$$u_m(t) = i_m(t)R_m + \frac{\mu_0 N_m^2 A_m}{2x_m(t)}\frac{di_m(t)}{dt} - \frac{\mu_0 N_m^2 A_m i_m(t)}{2x_m^2(t)}\frac{dx_m(t)}{dt} \tag{8}$$

Assuming f_d is the disturbance force of the suspension electromagnet (such as: wind force, force generated by sudden changes in the power grid, etc.), the dynamic equation of the suspension system in the vertical direction is described as follows:

$$m\frac{d^2x_m(t)}{dt^2} = -\frac{\mu_0 A_m N_m^2}{4}\left[\frac{i_m(t)}{x_m(t)}\right]^2 + mg + f_d \tag{10}$$

Convert Eqs. (8) and (10) to state space expressions. Here, the system state is $x_1(t) = x_m(t)$, $x_2(t) = \dot{x}_m(t)$ and $y_3(t) = i_m(t)$ and the state space expression of the floating system is:

$$\begin{cases} \dot{x}_1(t) = x_2(t) \\ \dot{x}_2(t) = -\frac{\mu_0 A_m N_m^2}{4m}\left[\frac{x_3(t)}{x_1(t)}\right]^2 + g + \frac{1}{m}f_d \\ \dot{x}_3(t) = \frac{x_2(t)x_3(t)}{x_1(t)} + \frac{2x_1(t)}{\mu_0 N_m^2 A_m}(u_m(t) - x_3(t)R_m) \\ y(t) = x_1(t) \end{cases} \tag{11}$$

3. Control strategy design based on neural network minimum parameter learning

3.1. Affine nonlinear mathematical model

In order to obtain the affine nonlinear mathematical model of the maglev system, according to the principle of nonlinear coordinate transformation, the nonlinear transformation coordinate is selected as follow:

$\boldsymbol{\eta} = [z_1 \quad z_2 \quad z_3]^T \in \Omega_\eta, \Omega_\eta \in R^3$ is a compact set in R^3.

where,

$$\begin{cases} z_1 = x_1 \\ z_2 = x_2 \\ z_3 = g - \frac{\mu_0 A_m N_m^2}{4m}\left(\frac{x_3}{x_1}\right)^2 \end{cases} \tag{12}$$

Further, it is not difficult to obtain:

$$\begin{cases} \dot{z}_1 = z_2 \\ \dot{z}_2 = z_3 \\ \dot{z}_3 = -\frac{\mu_0 A_m N_m^2}{2m}\left(\frac{x_3\dot{x}_3}{x_1^2}\right) + \frac{\mu_0 A_m N_m^2}{2m}\left(\frac{x_3^2\dot{x}_1}{x_1^2}\right) \end{cases} \tag{13}$$

In order to facilitate the subsequent design, we define k and L:

$$k = \frac{\mu_0 A_m N_m^2}{4},\quad L = \frac{2k}{x_1}$$

According to the (1), $\dot{\eta}_3(t)$ can be written as:

$$\dot{z}_3 = \frac{2k}{m}\left(\left(1 - \frac{2k}{Lx_1}\right)\frac{x_2x_3^2}{x_1^3} + \frac{R_m}{L}\frac{x_3^2}{x_1^2}\right) - \frac{2kx_3}{Lmx_1^2}u_m \tag{14}$$

Therefore, the affine nonlinear mathematical model of the new coordinate system is developed as follows:

$$\begin{cases} \dot{z}_1 = z_2 \\ \dot{z}_2 = z_3 \\ \dot{z}_3 = f(\boldsymbol{x}) + g(\boldsymbol{x})u_m \\ y = z_1 \end{cases} \tag{15}$$

where,

$$f(\boldsymbol{x}) = \frac{2k}{m}\left(\left(1 - \frac{2k}{Lx_1}\right)\frac{x_2x_3^2}{x_1^3} + \frac{R}{L}\frac{x_3^2}{x_1^2}\right)$$

$$g(\boldsymbol{x}) = -\frac{2kx_3}{Lmx_1^2}$$

3.2. Preliminary design of sliding mode control law

The state variables of the maglev system are selected as:

$$z_1 = x_1 = x_m,\quad z_2 = x_2 = \dot{x}_m(t) \tag{16}$$

The system error and the rate of error can be defined as:

$$e = z_1 - r \tag{17}$$

where, r denotes a given desired position.

Based on (5), the sliding mode surface is designed as follow:

$$s \triangleq \{(e,\dot{e},\ddot{e}) | c_1e + c_2\dot{e} + \ddot{e} = 0\} \tag{18}$$

where, $c_1, c_2 \in R^+$ is the positive control gain. By utilizing (17), $e = z_1 - r = x_1 - r$.

The derivation of (18) is calculated as:

$$\begin{aligned} \dot{s} &= c_1(\dot{x}_1 - \dot{r}) + c_2(\ddot{x}_1 - \ddot{r}) + (\dddot{x}_1 - \dddot{r}) \\ &= f(\boldsymbol{x}) + g(\boldsymbol{x})u_m - \dddot{r} + c_1\dot{e} + c_2\ddot{e} \end{aligned} \tag{19}$$

By utilizing the exponential reaching law (i.e., $\dot{s} = -\eta sgn(s) - \mu s$), the sliding mode variable structure control law can be developed as follows:

$$u_{SMC}(\boldsymbol{x},t) = \frac{1}{g(\boldsymbol{x})}\left[-f(\boldsymbol{x}) + \dddot{r} - c_1\dot{e} - c_2\ddot{e} - \eta sgn(s) - \mu s\right] \tag{20}$$

where, η, $\mu \in R^+$ denote constant reaching coefficient and exponential reaching coefficient, respectively.

Lyapunov function is defined as:

$$V(x) = \frac{1}{2}s^2 \tag{21}$$

This function is positive semi-definite, and the derivative of the both side can be obtained as:

$$\begin{aligned}\dot{V}(x) &= s \cdot \dot{s} = -s \cdot \eta sgn(s) - \mu \cdot s^2 \\ &= -\eta|s| - \mu \cdot s^2 \leqslant 0\end{aligned} \tag{22}$$

Based on the Lyapunov theorem, it is easy to prove that the system is global asymptotically stable.

The method is based on the exact model. When $f(\cdot), g(\cdot)$ is uncertain or even unknown, the method is no longer applicable. RBF neural network can be used to learn and approximate $f(\cdot), g(\cdot)$ online.

3.3. RBF neural network minimum parameter learning method

For the complex model information in magnetic levitation system, the traditional RBF network is used for approximation as shown in Fig. 3, which can realize the adaptive control of neural network without model information, but the algorithm is not good for real-time control [34–37]. The minimum parameter learning method is adopted to replace the weights in the neural network without model information, and the adaptive control based on the minimum parameter estimation is realized, thereby improving the convergence speed of the adaptive algorithm and better meeting the requirements of real-time control.

By utilizing the RBF neural network to learn and approximate $f(\cdot)$ and $g(\cdot)$, the closed-loop control system can be shown in Fig. 4:

The input and output algorithm of RBF neural network is

$$h_j = \exp\left(\frac{\| \boldsymbol{x} - \boldsymbol{c}_j \|^2}{2b_j^2}\right) \tag{23}$$

$$f(\boldsymbol{x}) = \boldsymbol{W}^{*T}\boldsymbol{h}_f(\boldsymbol{x}) + \varepsilon_f, \quad g(\boldsymbol{x}) = \boldsymbol{L}^{*T}\boldsymbol{h}_g(\boldsymbol{x}) + \varepsilon_g \tag{24}$$

where, $\boldsymbol{x}$ is the input of the neural network, j is the j node of the hidden layer, $\boldsymbol{h} = [h_j]^{\mathrm{T}}$ is the output of the Gaussian basis function, d a n d e are the ideal weights of the approximated network, f a n d g are the approximation errors of the network respectively. $\boldsymbol{W}^*, \boldsymbol{L}^*$ are the ideal network weights of $f(\cdot), g(\cdot)$ respectively, and $\varepsilon_f, \varepsilon_g$ are network approximation errors respectively, $|\varepsilon_f| \leqslant \varepsilon_{Mf}$, $|\varepsilon_g| \leqslant \varepsilon_{Mg}$

When $\boldsymbol{x} = [x_1 \quad x_2 \quad x_3]^{\mathrm{T}}$ is set, the RBF output is:

$$\hat{f}(\boldsymbol{x}) = \hat{\boldsymbol{W}}^{\mathrm{T}}\mathbf{h}_{\mathrm{f}}(\mathbf{x}), \hat{\mathrm{g}}(\mathbf{x}) = \hat{\mathbf{L}}^{\mathrm{T}}\mathbf{h}_{\mathrm{g}}(\mathbf{x}) \tag{25}$$

Among them, $\boldsymbol{h}_f(\boldsymbol{x})$ and $\boldsymbol{h}_g(\boldsymbol{x})$ are the Koski functions of RBF neural network.

The minimum parameter learning method of neural network is used for $f(\cdot)$ and $g(\cdot)$ respectively. Let $\phi = \| \boldsymbol{W}^* \|^2$, ϕ is a positive real number, $\hat{\phi}$ is ϕ's online estimation value, learning error is $\tilde{\phi} = \hat{\phi} - \phi$. Let $\varphi = \| \boldsymbol{L}^* \|^2$, φ is a positive real number, $\hat{\varphi}$ is φ's online estimation value, learning error is $\tilde{\varphi} = \hat{\varphi} - \varphi$.

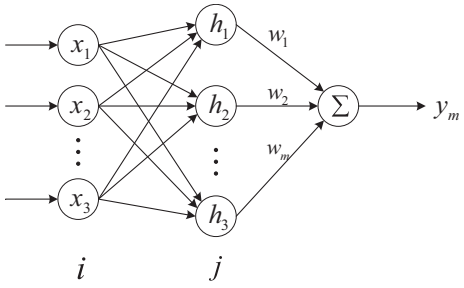

Fig. 3. The structure of RBF Neural Network.

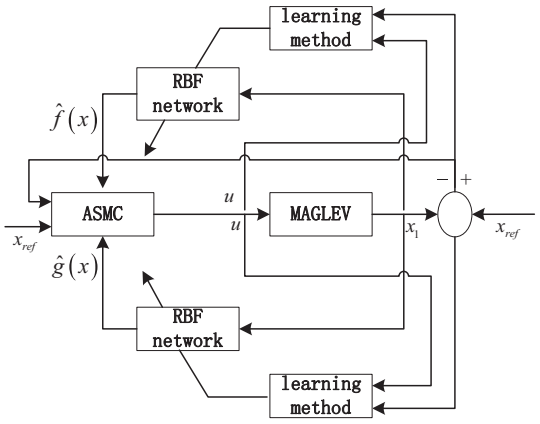

Fig. 4. Block diagram of the overall control scheme.

The design control law is as follows:

$$u_m(\boldsymbol{x}, t) = \frac{1}{1/2s\hat{\varphi}\boldsymbol{h}_g^{\mathrm{T}}\mathbf{h}_{\mathrm{g}}}\left[-\frac{1}{2}s\hat{\phi}\boldsymbol{h}_f^{\mathrm{T}}\mathbf{h}_{\mathrm{f}} + \dddot{\mathrm{r}} - \mathrm{c}_1\dot{\mathrm{e}} - \mathrm{c}_2\ddot{\mathrm{e}} - \eta sgn(\mathrm{s}) - \mu s\right] \tag{26}$$

where, $sgn(\cdot)$ is the signum function, and s denotes the dynamic sliding surface defined by (18), and $\mu > 0$.

According to the minimum parameter learning method, the adaptive laws are designed for single parameter $\hat{\phi}$ and $\hat{\varphi}$ of $f(\cdot)$ and $g(\cdot)$ respectively.

$$\dot{\hat{\phi}} = \frac{\gamma_1}{2}s^2\boldsymbol{h}_f^{\mathrm{T}}\mathbf{h}_{\mathrm{f}} - \Omega_1\gamma_1\hat{\phi} \tag{27}$$

$$\dot{\hat{\varphi}} = \frac{\gamma_2}{2}s^2\boldsymbol{h}_g^{\mathrm{T}}\mathbf{h}_{\mathrm{g}}\mathrm{u}_{\mathrm{m}} - \Omega_2\gamma_2\hat{\varphi} \tag{28}$$

$$\gamma_1\gamma_2\Omega_1\Omega_2 \in R^+$$

4. Convergence proof

Substituting the controller (26) into $\dot{s}$, we can obtain equation as follows:

$$\begin{aligned}\dot{s} &= f(\boldsymbol{x}) + \hat{g}(\boldsymbol{x})u_m + (g(\boldsymbol{x}) - \hat{g}(\boldsymbol{x}))u_m - \dddot{r} + c_1\dot{e} + c_2\ddot{e} \\ &= f(\boldsymbol{x}) + \hat{g}(\boldsymbol{x})\frac{1}{\hat{g}(\boldsymbol{x})}\left[-\frac{1}{2}s\hat{\phi}\boldsymbol{h}_f^{\mathrm{T}}\mathbf{h}_{\mathrm{f}} + \dddot{\mathrm{r}} - \mathrm{c}_1\dot{\mathrm{e}} - \mathrm{c}_2\ddot{\mathrm{e}} - \eta sgn(\mathrm{s}) - \mu s\right] \\ &\quad + (g(\boldsymbol{x}) - \hat{g}(\boldsymbol{x}))u_m - \dddot{r} + c_1\dot{e} + c_2\ddot{e} \\ &= \boldsymbol{W}^{*T}\boldsymbol{h}_f(\boldsymbol{x}) + \varepsilon_f - \frac{1}{2}s\hat{\phi}\boldsymbol{h}_f^{\mathrm{T}}\mathbf{h}_{\mathrm{f}} - \eta sgn(\mathrm{s}) - \mu s + (\mathbf{L}^{*\mathrm{T}}\mathbf{h}_{\mathrm{g}}(\mathbf{x}) \\ &\quad + \varepsilon_{\mathrm{g}} - \frac{1}{2}\mathrm{s}\hat{\varphi}\mathbf{h}_{\mathrm{g}}^{\mathrm{T}}\mathbf{h}_{\mathrm{g}})\mathrm{u}_{\mathrm{m}}\end{aligned} \tag{29}$$

The Lyapunov function is defined as:

$$V = \frac{1}{2}s^2 + \frac{1}{2\gamma_1}\tilde{\phi}^2 + \frac{1}{2\gamma_2}\tilde{\varphi}^2 \tag{30}$$

It can be obtained that:

$$V \geqslant 0 \tag{31}$$

$$\begin{aligned}\dot{V} &= s\dot{s} + \frac{1}{\gamma_1}\tilde{\phi}\dot{\hat{\phi}} + \frac{1}{\gamma_2}\tilde{\varphi}\dot{\hat{\varphi}} \\ &= s(\boldsymbol{W}^{*T}\boldsymbol{h}_f(\boldsymbol{x}) + \varepsilon_f - \frac{1}{2}s\hat{\phi}\boldsymbol{h}_f^{\mathrm{T}}\mathbf{h}_{\mathrm{f}} - \eta sgn(\mathrm{s}) - \mu s + (\mathbf{L}^{*\mathrm{T}}\mathbf{h}_{\mathrm{g}}(\mathbf{x}) \\ &+ \varepsilon_{\mathrm{g}} - \frac{1}{2}\mathrm{s}\hat{\varphi}\mathbf{h}_{\mathrm{g}}^{\mathrm{T}}\mathbf{h}_{\mathrm{g}})\mathrm{u_m}) + \frac{1}{\gamma_1}\tilde{\phi}\dot{\hat{\phi}} + \frac{1}{\gamma_2}\tilde{\varphi}\dot{\hat{\varphi}}\end{aligned} \tag{32}$$

Note 1: the following two conclusions are used in the proof:

$$\begin{aligned}s^2\phi\boldsymbol{h}_f^{\mathrm{T}}\mathbf{h}_{\mathrm{f}} + 1 &= s^2\|\mathbf{W}^*\|^2\mathbf{h}_{\mathrm{f}}^{\mathrm{T}}\mathbf{h}_{\mathrm{f}} + 1 = s^2\|\mathbf{W}^*\|^2\|\mathbf{h}_{\mathrm{f}}\|^2 + 1 \\ &= s^2\|\mathbf{W}^{*\mathrm{T}}\mathbf{h}_{\mathrm{f}}\|^2 + 1 \geqslant 2s\mathbf{W}^{*\mathrm{T}}\mathbf{h}_{\mathrm{f}}\end{aligned}$$

$$\text{that is, } s\mathbf{W}^{*\mathrm{T}}\mathbf{h}_{\mathrm{f}} \leqslant \frac{1}{2}s^2\phi\mathbf{h}_{\mathrm{f}}^{\mathrm{T}}\mathbf{h}_{\mathrm{f}} + \frac{1}{2} \tag{33}$$

$$\text{Similarly, } s\mathbf{L}^{*\mathrm{T}}\mathbf{h}_{\mathrm{g}} \leqslant \frac{1}{2}s^2\varphi\mathbf{h}_{\mathrm{g}}^{\mathrm{T}}\mathbf{h}_{\mathrm{g}} + \frac{1}{2} \tag{34}$$

$$\begin{aligned}\dot{V} &\leqslant \tfrac{1}{2}s^2\phi\boldsymbol{h}_f^{\mathrm{T}}\mathbf{h}_{\mathrm{f}} + \tfrac{1}{2} - \tfrac{1}{2}s^2\hat{\phi}\mathbf{h}_{\mathrm{f}}^{\mathrm{T}}\mathbf{h}_{\mathrm{f}} + (\varepsilon_{\mathrm{f}} + \varepsilon_{\mathrm{g}}\mathrm{u_m})\mathrm{s} - \eta|\mathrm{s}| - \mu s^2 \\ &+\left(\tfrac{1}{2}s^2\varphi\mathbf{h}_{\mathrm{g}}^{\mathrm{T}}\mathbf{h}_{\mathrm{g}} + \tfrac{1}{2} - \tfrac{1}{2}s^2\hat{\varphi}\mathbf{h}_{\mathrm{g}}^{\mathrm{T}}\mathbf{h}_{\mathrm{g}}\right)\mathrm{u_m} + \tfrac{1}{\gamma_1}\tilde{\phi}\dot{\hat{\phi}} + \tfrac{1}{\gamma_2}\tilde{\varphi}\dot{\hat{\varphi}} \\ &= -\tfrac{1}{2}s^2\tilde{\phi}\boldsymbol{h}_f^{\mathrm{T}}\mathbf{h}_{\mathrm{f}} + \tfrac{1}{2} + (\varepsilon_{\mathrm{f}} + \varepsilon_{\mathrm{g}}\mathrm{u_m})\mathrm{s} - \eta|\mathrm{s}| - \mu s^2 \\ &+\left(\tfrac{1}{2} - \tfrac{1}{2}s^2\tilde{\varphi}\mathbf{h}_{\mathrm{g}}^{\mathrm{T}}\mathbf{h}_{\mathrm{g}}\right)\mathrm{u_m} + \tfrac{1}{\gamma_1}\tilde{\phi}\dot{\hat{\phi}} + \tfrac{1}{\gamma_2}\tilde{\varphi}\dot{\hat{\varphi}} \\ &= \tilde{\phi}\left(\tfrac{1}{\gamma_1}\dot{\hat{\phi}} - \tfrac{1}{2}s^2\boldsymbol{h}_f^{\mathrm{T}}\mathbf{h}_{\mathrm{f}}\right) + \tfrac{1}{2} + \tilde{\varphi}\left(\tfrac{1}{\gamma_2}\dot{\hat{\varphi}} - \tfrac{1}{2}s^2\boldsymbol{h}_{\mathrm{g}}^{\mathrm{T}}\mathbf{h}_{\mathrm{g}}\mathrm{u_m}\right) \\ &+(\varepsilon_f + (\varepsilon_g + 0.5)u_m)s - \eta|s| - \mu s^2\end{aligned}$$

Because RBF network approximation error ε_f and ε_g are very small real numbers, by choosing $\eta \geqslant |\varepsilon_f + (\varepsilon_g + 0.5)u_m|$, the $\dot{V}$ can be rewritten as follows:

$$\dot{V} \leqslant \tilde{\phi}\left(\frac{1}{\gamma_1}\dot{\hat{\phi}} - \frac{1}{2}s^2\boldsymbol{h}_f^{\mathrm{T}}\mathbf{h}_{\mathrm{f}}\right) + \frac{1}{2} + \tilde{\varphi}\left(\frac{1}{\gamma_2}\dot{\hat{\varphi}} - \frac{1}{2}s^2\boldsymbol{h}_{\mathrm{g}}^{\mathrm{T}}\mathbf{h}_{\mathrm{g}}\mathrm{u_m}\right) - \mu s^2 \tag{35}$$

Substituting adaptive laws into available information:

$$\begin{aligned}\dot{V} &\leqslant -\Omega_1\tilde{\phi}\hat{\phi} + \frac{1}{2} - \Omega_2\tilde{\varphi}\hat{\varphi} - \mu s^2 \leqslant -\frac{\Omega_1}{2}\left(\tilde{\phi}^2 - \phi^2\right) \\ &- \frac{\Omega_2}{2}\left(\tilde{\varphi}^2 - \varphi^2\right) + \frac{1}{2} - \mu s^2 \\ &= -\frac{\Omega_1}{2}\tilde{\phi}^2 - \frac{\Omega_2}{2}\tilde{\varphi}^2 - \mu s^2 + \left(\frac{\Omega_1}{2}\phi^2 + \frac{\Omega_2}{2}\varphi^2 + \frac{1}{2}\right)\end{aligned} \tag{36}$$

where, $\Omega_1 = \frac{2\mu}{\gamma_1}$, $\Omega_2 = \frac{2\mu}{\gamma_2}$

It can be obtained as follows:

$$\begin{aligned}\dot{V} &\leqslant -\frac{\mu}{\gamma_1}\tilde{\phi}^2 - \frac{\mu}{\gamma_2}\tilde{\varphi}^2 - \mu s^2 + \left(\frac{\Omega_1}{2}\phi^2 + \frac{\Omega_2}{2}\varphi^2 + \frac{1}{2}\right) \\ &= -2\mu\left(\frac{1}{2}s^2 + \frac{1}{2\gamma_1}\tilde{\phi}^2 + \frac{1}{2\gamma_2}\tilde{\varphi}^2\right) + \left(\frac{\Omega_1}{2}\phi^2 + \frac{\Omega_2}{2}\varphi^2 + \frac{1}{2}\right) \\ &= -2\mu V + R\end{aligned}$$

where, $R = \frac{\Omega_1}{2}\phi^2 + \frac{\Omega_2}{2}\varphi^2 + \frac{1}{2}$

Solving inequality $\dot{V} \leqslant -2\mu V + R$, we can learn that as follows:

$$V \leqslant \frac{R}{2\mu} + \left(V(0) - \frac{R}{2\mu}\right)e^{-2\mu t} \tag{37}$$

$$\begin{aligned}\lim_{t\to\infty} V &= \frac{R}{2\mu} = \frac{\frac{\Omega_1}{2}\phi^2 + \frac{\Omega_2}{2}\varphi^2 + \frac{1}{2}}{2\mu} = \frac{\Omega_1\phi^2 + \Omega_2\varphi^2 + 1}{4\mu} \\ &= \frac{\frac{2\mu}{\gamma_1}\phi^2 + \frac{2\mu}{\gamma_2}\varphi^2 + 1}{4\mu} = \frac{\phi^2}{2\gamma_1} + \frac{\varphi^2}{2\gamma_2} + \frac{1}{4\mu}\end{aligned} \tag{38}$$

It can be seen that the system is ultimately uniformly bounded. Therefore, the boundedness and convergence of the system are proved. The neural network weights $\hat{\boldsymbol{W}}$ and $\hat{\boldsymbol{L}}$ are transformed into single parameters $\hat{\phi}$ and $\hat{\varphi}$ respectively, which speeds up the solution of the adaptive law and the learning and convergence speed of the controller.

5. Simulation results

The numerical simulation is executed to analyze and evaluate the performance of the designed controller (RBF MPL-ASMC) using the similar design parameter values as of the test maglev train. The parameters of the maglev system are based on the test maglev bogie of the low-speed maglev train at the national maglev center. The initial position of the suspension airgap is 0.017 m, and the target position of the airgap is 0.009 m. The MATLAB/SIMULINK platform is utilized to simulate the adaptive sliding mode control based on RBF neural network minimum parameter learning method (RBF MPL-ASMC), which is used for comparison with the traditional linear PID. For the RBF network, the value of c_j is 0.45 and b_j is 8. The initial weight values of RBF neural network are all set to 0.10. The parameters of the maglev system are listed in Table.1.

The controller parameters are sufficiently tuned to obtain the best performance. The control law is designed by utilizing (26). In the sliding mode function, $c_1 = 1, c_2 = 10\eta = 0.5\mu = 1$. The minimum parameter learning law is designed using (27) and (28). Adaptive parameters γ_1, γ_2 are all set to 0.2.

Fig. 5 shows the step response of the maglev system under the action of the designed controller. An unmodeled dynamic of 140sin (t) is added to the system model. If not controlled by the controller, this disturbance will produce an maximum acceleration of 0.2 m/s^2. Fig. 6 shows the response of the control current.

Fig. 7 shows the plot of the $f(\cdot)$ and $\hat{f}(\cdot)$ learning estimation processes, and Fig. 8 shows the image of the $g(\cdot)$ and its estimate $\hat{g}(\cdot)$. It can be seen that the algorithm proposed in this paper can learn and approximate the true value very quickly. Add the unmodeled dynamics of 420sin (10πt) to the model, the air gap response and current response of the designed controller are shown in Figs. 9 and 10, respectively. And Phase locus of the system with 420sin (10πt) as the unmodeled dynamics is shown in Fig. 11. Fig. 12 shows a phase locus when 1680sin (10πt) are incorporated into the system as the non-modeled dynamics. The phase locus slides along the sliding surface, and the slope of the sliding surface is −10, which is equal to the value of c_2/c_1.

In order to analyze the performance of the proposed controller, the performance of the proposed adaptive controller was compared with classical control. For this purpose, a PID controller is designed for the linearization model of the magnetic levitation system based on the method proposed in [29].The parameters of the PID controller for the magnetic levitation system are Kp = 7000, ki = 900, kd = 1100.

In order to verify the anti-disturbance capability of the proposed controller, a constant interference force of 2kN is added to

Table 1
Parameter values of the levitation system.

Physical quantity	Value	Physical quantity	Value
Mass m/kg	700	Leakage permeance η	0
Number of turns of coil N_m	450	Permeability of air $\mu_0/(H\cdot m^{-1})$	$4\pi\times10^{-7}$
Cross sectional area of Magnet A_m/m^2	0.024	Nominal current i_{ref}/A	19.1
coil resistance R_m/Ω	1.2	Nominal airgap x_{ref}/m	0.009

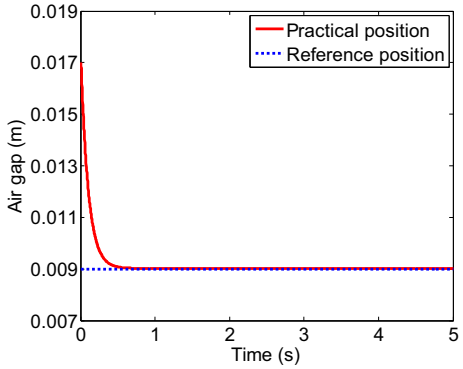

Fig. 5. Air gap response of the Maglev system with the proposed controller.

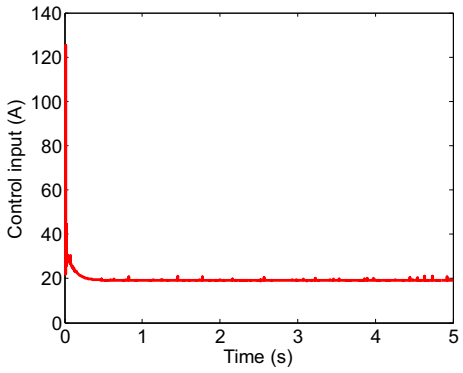

Fig. 6. Control current for the Maglev.

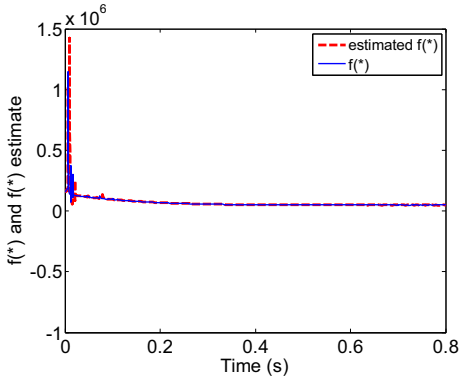

Fig. 7. $f(\cdot)$ and its estimate $\hat{f}(\cdot)$.

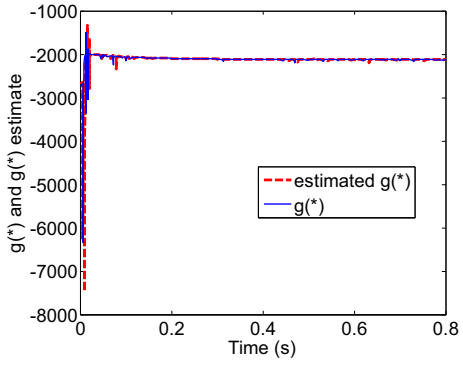

Fig. 8. $g(\cdot)$ and its estimate $\hat{g}(\cdot)$.

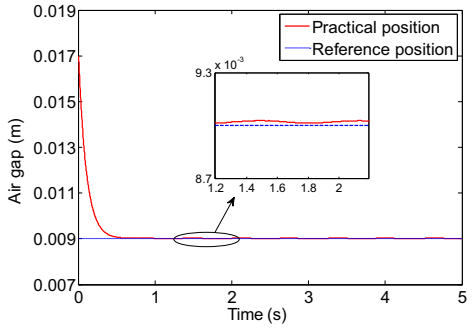

Fig. 9. Air gap response with 420sin (10πt) as unmodeled dynamics.

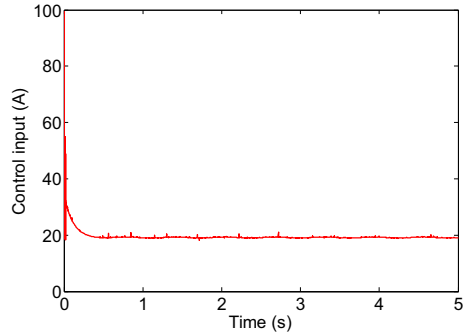

Fig. 10. Current response with 420sin (10πt) as unmodeled dynamics.

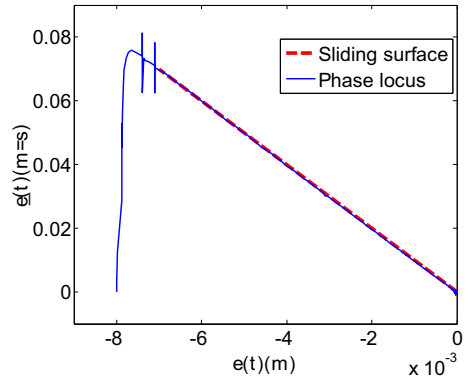

Fig. 11. Phase locus of the system with 420sin (10πt) as the unmodeled dynamics.

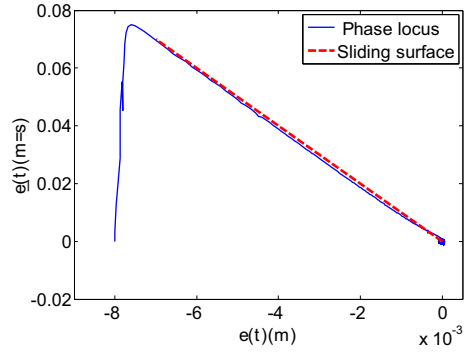

Fig. 12. Phase locus of the system with 1680sin (10πt) as the unmodeled dynamics.

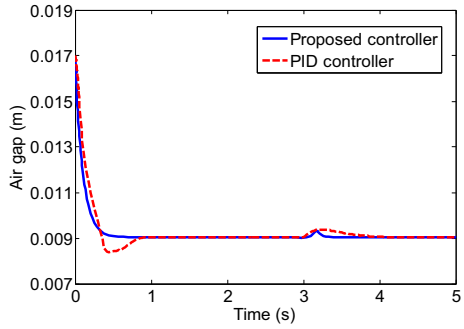

Fig. 13. Response of constant disturbance force rejection comparison of PID.

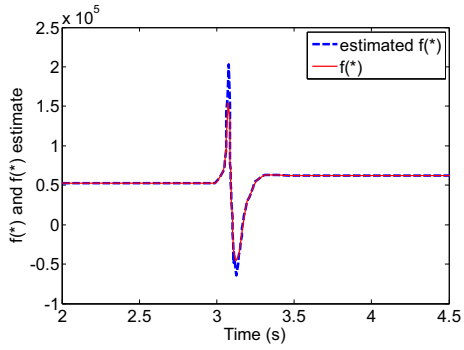

Fig. 14. $f(\cdot)$ and its estimate $\hat{f}(\cdot)$ with constant disturbance force.

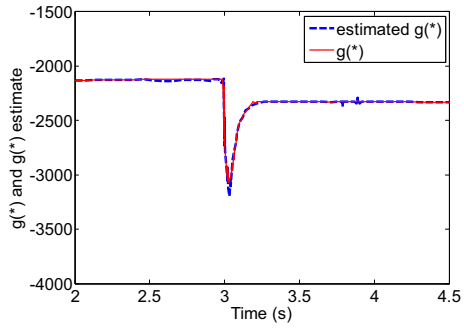

Fig. 15. $g(\cdot)$ and its estimate $\hat{g}(\cdot)$ with constant disturbance force.

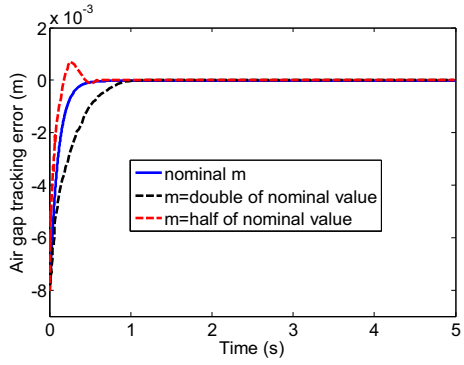

Fig. 16. Response of the maglev system with the comparison of PID.

the system when t = 3. The resulting response of the proposed controller and the PID controller are all shown in Fig. 13. The proposed controller has significantly better interference suppression capability than the traditional PID controller. The designed adaptive controller is very good for system dynamic evaluation. As shown in Figs. 14 and 15, at time = 3 s when the constant interference is applied.

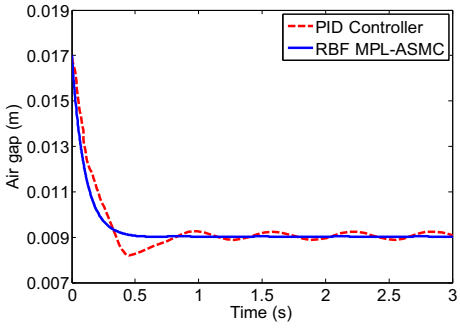

Fig. 17. Response with unmodeled dynamics added to the system

To evaluate the robustness of the designed controller, the physical parameter values of the magnetic levitation system vary between half and two times the nominal value. The simulated output response of maglev system remained bounded for the variation in parameters. Fig. 16 shows the air gap response with the mass of train being doubled and halved of the nominal value. Similar analysis was implemented for R_m, A_m, N_m and the air gap remained bounded for parameters perturbations.

In order to simulate the condition of track irregularity, sinusoidal disturbance with different frequencies is added to the system. Fig. 17 shows a comparison of the PID controller and the proposed controller for 10 Hz low frequency interference for the position tracking of the maglev system. Under the action of PID, the deviation between air gap and reference value is up to 5.6%. However the sinusoidal disturbance effect exists with an amplitude of 0.16% of the reference air gap under the proposed RBF MPL-ASMC controller, as shown in Fig. 17. It can be seen that the RBF MPL-ASMC controller has more advantages than the traditional PID when dealing with the track irregularity.

6. Experimental results

After the numerical simulations, significant efforts are made to implement the experiments with the aim of examining the practical performance of the proposed control scheme. The experiments are implemented in the national low-speed maglev test line. The full-scale test maglev bogie of 4 electromagnet coils is shown in Fig. 18. The maglev train uses the eddy current sensor to measure the air gap. Due to the eddy current effect, the change of the displacement amount will affect the impedance value of the sensor coil, and the signal measurement circuit converts the changed impedance value into a corresponding voltage signal, thereby obtaining the air gap data.

The reference levitation airgap of maglev system during operation is set to 9 mm, and the initial airgap is 17 mm. The sampling frequency is 2500 Hz, and the experimental parameters of the system and the parameters of the RBF MPL-ASMC are consistent with the parameters used in the theoretical analysis and simulation. Experiments are carried out to analyze and verify the proposed RBF MPL-ASMC over the widely used PID controller.

To fully investigate the performance of the presented control scheme, two sets of experiments are carried out to examine the tracking performance, and the disturbance rejection capacity, respectively. The control parameters values in the experiment are consistent with the simulation.

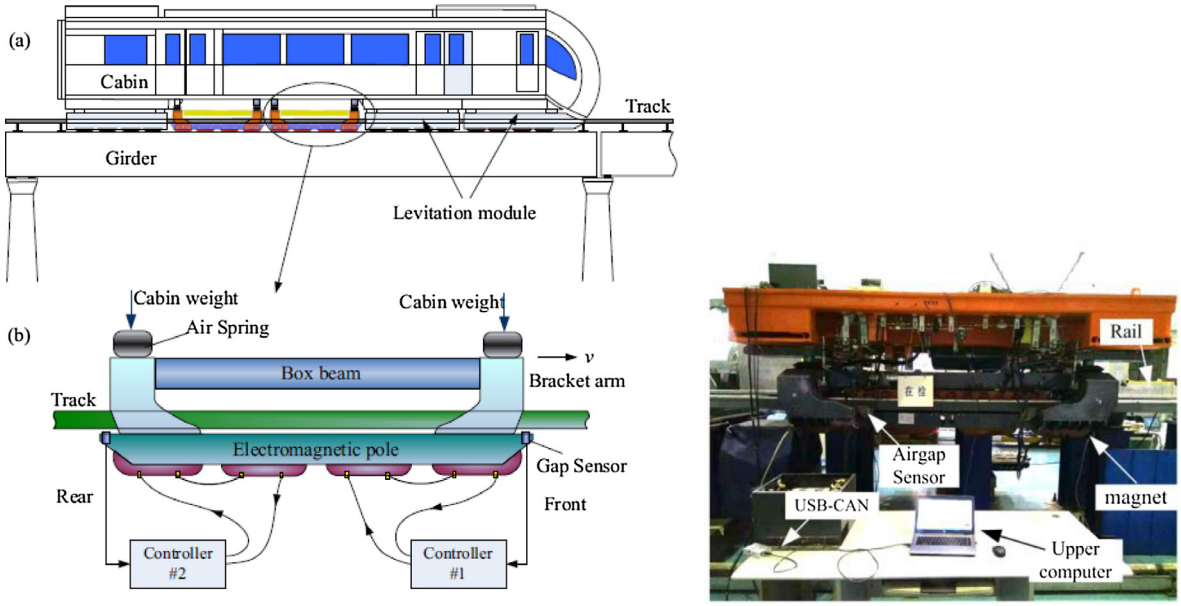

Fig. 18. The full-scale test maglev bogie of 4 electromagnet coils.

Experiment 1: The first experiment is utilized to examine the tracking performance of the proposed RBF MPL-ASMC control scheme. The maglev bogie stays at the initial position of 17 mm. From the time $t = 0$ s, the control law is employed to drive the train to the desired position of $r = 9$ mm.

Experiment 2: Dynamic disturbance response analysis. External disturbance signal is imposed: the train is levitated under the disturbance signal shown in Fig. 21 (periodic disturbance).

During the operation of maglev system levitation, it is unavoidable to encounter the situation that the gravity in the carriage suddenly increases or decreases during the passengers boarding or alighting. Because the maglev train has a small levitation airgap during the stable operation, the excessive gravity change is easy to cause the train break down or lose its stability. When the disturbance signal is applied to the maglev system, the sliding rack of the maglev bogie contacted the guideway, which means the controller loses its stability under the disturbance.

The airgap resulting response with the RBF MPL-ASMC controller proposed in this paper is shown in Fig. 21. It can be seen from the Fig. 21 that the proposed controller can still be levitated steadily under the external disturbance.

The experimental results in two cases are given by Figs. 19–22 respectively. According to Figs. 19 and 20, in the case of static levitation, the conventional PID controller cannot obtain the ideal PID parameters because of the limitation of manual adjustment of PID parameters. So it can only rely on experience to determine the value, which determines that the tracking performance is weaker

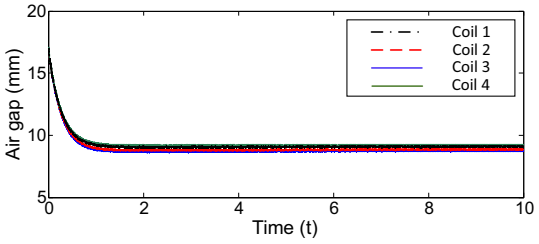

Fig. 20. Multi coil suspension airgap under RBF MPL-ASMC.

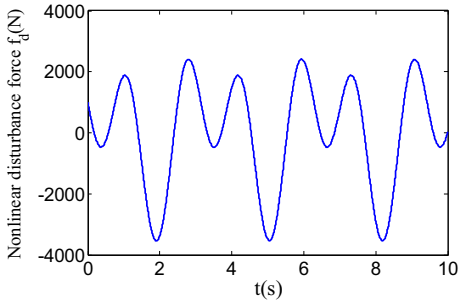

Fig. 21. Periodic disturbance signal.

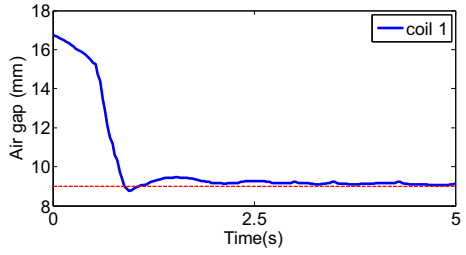

Fig. 19. Air gap under PID.

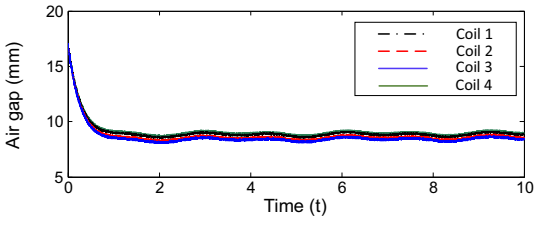

Fig. 22. Multi coil suspension airgap under RBF NMPL-ASMC.

than the RBF NMPL-ASMC controller proposed in this paper. When the disturbance signal like Fig. 21 is added to the system, the PID controller loses stability and cannot realize the levitation. But the RBF NMPL-ASMC controller can realize the stable levitation of the maglev train. The proposed control law has strong robustness, tracking performance and strong anti-disturbance ability. In addition, the RBF NMPL-ASMC controller is more robust than the PID controller under multi-coil coupling effect in real-time. Moreover, as shown in Fig. 22, the proposed controller can remove the influence of vertical load change and realize more stable levitation, as shown in Fig. 22, which can effectively eliminate the influence of passengers boarding or alighting effect on the train and ensure the stable levitation of the train. So it can be concluded that although the gravity change will still have an effect on the suspension air gap, but the change is small and smooth. Compared with the traditional PID controller, the proposed controller can maintain the suspension performance more effectively and improve the levitation performance under the coupling multi-electromagnet coils.

7. Conclusion

In this paper, an adaptive sliding mode control law based on RBF neural network minimum parameter learning method (RBF MPL-ASMC) is designed for maglev train. As we know, when the parameters of the maglev system change, the traditional PID controller has a slower response speed, a large overshoot, and chattering, which reduces stability and robustness of the system. In order to solve these problems, RBF neural network with minimum parameter learning method is applied to the sliding mode control of maglev system. SMC control and RBF neural network with minimum parameter learning method are combined to develop a better real-time controller for maglev system deal with unmodeled dynamics and unexpected disturbance. This algorithm makes maglev systems levitate stably, and has faster response speed and stronger robustness when the model parameters change and external disturbances exist. The minimum parameter learning method improved the convergence speed of the proposed control algorithm and better meeting the requirements of real-time control. Through the experimental platform, the experimental results comparison of PID controller and RBF MPL-ASMC controller are included to verify the validity of the theoretical analysis and control method. However, there is no specific tune rule of control parameters setting. This will be the focus of further research. Moreover, due to the high rigidity of the existing magnetic levitation guideway, the study in this paper is based on the taking the guideway as a rigid body. Our future works will study the intelligent maglev control method with flexible guideway, which can reduce the requirement of guideway stiffness and thus greatly reduce the cost of the maglev guideway.

Acknowledgements

This work was supported in part by the National Key R&D Program of China “Research on Key Technologies of Maglev Transportation System” (2016YFB1200600) and the Fundamental Research Funds for the Central Universities.

References

[1] H.W. Lee, K.C. Kim, J. Lee, Review of maglev train technologies, IEEE Trans. Magn. 42 (7) (2006) 1917–1925.
[2] Y.G. Sun, W.L. Li, H.Y. Qiang, et al., An experimental study on the vibration of the low-speed maglev train moving on the guideway with sag vertical curves, Int. J. Control Autom. 9 (4) (2016) 279–288.
[3] R.D. Thornton, Efficient and affordable maglev opportunities in the United States, Proc. IEEE 97 (11) (2009) 1901–1921.
[4] I. Boldea, L. Tutelea, W. Xu, et al., Linear electric machines, drives and MAGLEVs: an overview, IEEE Trans. Ind. Electron. 65 (9) (2018) 7504–7515.
[5] X.M. Zhou, W.M. Liu, Key technologies in the construction of medium and low speed maglev in Changsha City, Urban Mass Transit. 19 (5) (2016) 1–4.
[6] R.J. Wai, J.D. Lee, Robust levitation control for linear maglev rail system using fuzzy neural network, IEEE Trans. Control Syst. Technol. 17 (1) (2009) 4–14.
[7] X.D. Zhang, M. Mehrtash, M.B. Khamesee, Dual-axial motion control of a magnetic levitation system using hall-effect sensors, IEEE-ASME Trans. Mechatron. 21 (2) (2016) 1129–1139.
[8] Z.Q. Long, A.M. Hao, W.S. Chang, Suspension controller design of maglev train considering the rail track periodical irregularity, J. Natl. Univ. Defense Technol. 25 (2) (2003) 84–89.
[9] J.D. Lindlau, C.R. Knospe, Feedback linearization of an active magnetic bearing with voltage control, IEEE Trans. Control Syst. Technol. 10 (1) (2002) 21–31.
[10] W.R. Song, G.F. Yu, Y.F. Wang, PID control of micro feed mechanism based on magnetic levitation technology, J. Harbin Inst. Technol. 36 (1) (2004) 28–31.
[11] L.M. Dai, B. Qi, H.B. Zhou, et al., PID control and experiment for magnetism levitation movement system, Mod. Manuf. Eng. 6 (2008) 79–82.
[12] Ning Sun, Tong Yang, Yongchun Fang, Wu Yiming, He Chen, Transportation control of double-pendulum cranes with a nonlinear quasi-PID scheme: design and experiments, IEEE Trans. Syst., Man, Cybern.: Syst. (2018), https://doi.org/10.1109/TSMC.2018.2871627, in press.
[13] Huimin Ouyang, Xin Deng, Huan Xi, Hu Jinxin, Guangming Zhang, Lei Mei, Novel robust controller design for load sway reduction in double-pendulum overhead cranes, Proc. Inst. Mech. Eng., Part C: J. Mech. Eng. Sci. (2018), https://doi.org/10.1177/0954406218813383.
[14] H.R. Jamshidi, A. Karimi, M. Haghshenas, Risk assessment of particulate matters in a dentistry school using fuzzy inference systems, Measurement 116 (2018) 257–263.
[15] H. Wang, X.B. Zhong, G. Shen, A new maglev line system design and control strategy, J. Tongji Univ. (Nat. Sci.) 41 (7) (2013) 1112–1118.
[16] X. Su, X. Yang, P. Shi, et al., Fuzzy control of nonlinear electromagnetic suspension systems, Mechatronics 24 (4) (2014) 328–335.
[17] S.J. Huang, W.C. Lin, Adaptive fuzzy controller with sliding surface for vehicle suspension control, IEEE Trans. Fuzzy Syst. 11 (4) (2003) 550–559.
[18] Y.G. Sun, H.Y. Qiang, X. Mei, et al., Modified repetitive learning control with unidirectional control input for uncertain nonlinear systems, Neural Comput. Appl. 30 (6) (2018) 2003–2012.
[19] Z.J. Yang, K. Kunitoshi, S. Kanae, et al., Adaptive robust output-feedback control of a magnetic levitation system by K-filter approach, IEEE Trans. Ind. Electron. 55 (1) (2008) 390–399.
[20] You-Gang Sun, Xu Jun-Qi, Chen Chen, Guo-Bin Lin, Fuzzy H∞ robust control for magnetic levitation system of maglev vehicles based on T-S fuzzy model: design and experiments, J. Intell. Fuzzy Syst. (2018), https://doi.org/10.3233/JIFS-169868.
[21] C.M. Huang, J.Y. Yen, M.S. Chen, Adaptive nonlinear control of repulsive maglev suspension systems, Control Eng. Pract. 8 (12) (2000) 1357–1367.
[22] H.M. Gutierrez, H. Luijten, 5-DOF real-time control of active electrodynamic maglev, IEEE Trans. Ind. Electron. 65 (9) (2018) 7468–7476.
[23] J. Xu, C. Chen, D. Gao, et al., Nonlinear dynamic analysis on maglev train system with flexible guideway and double time-delay feedback control, J. Vibroeng. 19 (8) (2017) 6346–6362.
[24] Y.G. Sun, W.L. Li, J.Q. Xu, et al., Nonlinear dynamic modeling and fuzzy sliding-mode controlling of electromagnetic levitation system of low-speed maglev train, J. Vibroeng. 19 (1) (2017) 328–342.
[25] J. Xu, Y. Sun, D. Gao, et al., Dynamic modeling and adaptive sliding mode control for a maglev train system based on a magnetic flux observer, IEEE Access 6 (2018) 31571–31579.
[26] J.C. Shen, H∞ control and sliding mode control of magnetic levitation system, Asian J. Control 4 (3) (2002) 333–340.
[27] H. Morioka, K. Wada, A. Sabanovic, et al., Neural network based chattering free sliding mode control, in: SICE '95. Proceedings of the, SICE Conference. International Session Papers, IEEE, 1995, pp. 1303–1308.
[28] S.J. Huang, K.S. Huang, K.C. Chiou, Development and application of a novel radial basis function sliding mode controller, Mechatronics 13 (4) (2003) 313–329.
[29] H.Y. Qiang, W.L. Li, Y.G. Sun, X.Y. Liu, Levitation chassis dynamic analysis and robust position control for maglev vehicles under nonlinear periodic disturbance, J. Vibroeng. 19 (2) (2017) 1273–1286.
[30] J.H. Li, J. Li, D.F. Zhou, et al., The active control of maglev stationary self-excited vibration with a virtual energy harvester, IEEE Trans. Ind. Electron. 62 (5) (2015) 2942–2951.
[31] Pan Yongping, Robust Adaptive Fuzzy Control for Nonlinear Systems (Ph.D. Dissertation), South China University of Technology, 2011.
[32] Y.G. Sun, J.M. Xie, J.Q. Xu, H.Y. Qiang, Design and control of simulation platform for low velocity maglev train magnetic levitation system, J. Mach. Des. 5 (2018) 14–19.
[33] Sun Yougang, Xu Junqi, Qiang Haiyan, Lin Guobin, Adaptive neural-fuzzy robust position control scheme for maglev train systems with experimental verification, IEEE Trans. Ind. Electron. (2019), https://doi.org/10.1109/TIE.2019.2891409.

[34] S. Brol, A. Szegda, Magnetism of automotive wheels with pneumatic radial tires, Measurement 126 (2018) 37–45.
[35] B. Jafarpisheh, S.M. Madani, F. Parvaresh, et al., Power system frequency estimation using adaptive accelerated MUSIC, IEEE Trans. Instrum. Meas. 99 (2018) 1–11.
[36] Y. Ege, M. Coramik, A new measurement system using magnetic flux leakage method in pipeline inspection, Measurement 123 (2018) 163–174.
[37] H. Cai, P. Li, C. Su, et al., Double-layered nonlinear model predictive control based on Hammerstein-Wiener model with disturbance rejection, Measur. Control 51 (7–8) (2018) 260–275.